Prediction of Semimetallic Tetragonal Hf_2O_3 and Zr_2O_3 from First Principles

Kan-Hao Xue,[1] Philippe Blaise,[2] Leonardo R. C. Fonseca,[3] and Yoshio Nishi[4]
[1]IMEP-LAHC, Minatec-INPG, 3 rue Parvis Louis Néel, BP 257, 38016 Grenoble Cedex 1, France
[2]CEA, LETI, Minatec Campus, 17 rue des Martyrs, 38054 Grenoble Cedex 9, France
[3]Center for Semiconductor Devices, State University of Campinas, Campinas, São Paulo, Brazil
[4]Department of Electrical Engineering, Stanford University, Stanford, California 94305, USA
(Received 1 November 2012; published 5 February 2013)

Tetragonal semimetallic phases are predicted for Hf_2O_3 and Zr_2O_3 using density functional theory. The structures belong to space group $P\bar{4}m2$ and are more stable than their corundum counterparts. Many body corrections at first order confirm their semimetallic character. The carrier concentrations are very similar for both materials, and are estimated as 1.8×10^{21} cm^{-3} for both electrons and holes, allowing for electric conduction. This could serve as a basic explanation for the low resistance state of hafnia-based resistive random access memory.

DOI: 10.1103/PhysRevLett.110.065502 PACS numbers: 61.50.Ah, 71.20.−b, 81.05.Bx, 81.05.Zx

Hafnia (HfO_2) and zirconia (ZrO_2) are found in a number of important technological applications [1,2]. In particular, hafnia has become a key component in submicrometer silicon MOS technology as the present choice of high permittivity dielectric layer [3]. In addition, it is also a promising candidate material for resistive random access memory (RRAM), which is one of the leading technologies for the next-generation nonvolatile memory [4–7]. The core element of RRAM is a metal-insulator-metal capacitor which is subject to an electroforming process, where a high electric field (some MV/cm) is applied across the capacitor to create conduction paths in the insulating thin film, here named filaments. These filaments are of unknown composition or shape, and can be easily disturbed under electrical stress, leading to a memory effect. Knowing the composition of the filaments is crucial to the understanding of RRAM's physics. Previous work on TiO_2 RRAM reveals that the conductive filament is possibly due to Ti_nO_{2n-1} Magnéli phases, where the value of n is mostly 4 or 5 [8]. For hafnia RRAM, the structure of the conductive filaments has not been reported, though it is widely accepted that the filaments are associated with an oxygen-deficient phase [9,10]. Since the impact of electroforming is expected to occur in small and random patches of the capacitor, experimental investigation of the filaments suffers from great difficulty.

In this Letter we employ first-principles density functional theory (DFT) [11] calculations to identify metallic O-poor stable compositions of hafnium and zirconium oxides, which may be reachable from room temperature normal pressure monoclinic Hf(Zr)O_2 [m-Hf(Zr)O_2] with the assistance of an external source of energy, possibly an applied electric field. While the processing and operation of oxide-based RRAM stimulated our search of a conductive phase in these materials, our predictions are quite general and should have broader implications in materials and device physics.

For our DFT calculations we employed the plane-wave-based Vienna *ab initio* simulation package (VASP) [12] with projector augmented-wave pseudopotentials [13] including Hf $5p$, $5d$, and $6s$ (Zr $4s$, $4p$, $4d$, and $5s$) electrons and O $2s$ and $2p$ electrons in the valence. Generalized gradient approximation (GGA) was used for the exchange-correlation energy, within the Perdew-Burke-Ernzerhof functional [14]. The plane-wave energy cutoff was chosen as 500 eV, which converged for all the involved compounds, and sufficiently dense Monkhorst-Pack [15] (Γ-centered for hcp structures) k mesh was utilized for sampling the Brillouin zone.

Since DFT-GGA usually underestimates band gaps [16], and may even deem a material metallic rather than semiconducting as in the case of bulk germanium [17], for the metal candidates we calculated the first order energy shifts with GW approximation [18] (G_0W_0) using the ABINIT [19,20] program. Hf (Zr) semicore electrons were explicitly included through the $5s^25p^65d^26s^2$ ($4s^24p^64d^25s^2$) configuration while core electrons were replaced by Troullier-Martins pseudopotentials [21]. Convergence was achieved with 360 bands and a 15 Ha cutoff for the wave functions employed in the evaluation of the dielectric function and the Σ function. A plasmon-pole approximation [22] was used.

The m-Hf(Zr)O_2 unit cells were fully relaxed until all Hellmann-Feynman forces were less than 0.01 eV/Å and all stresses were less than 400 MPa. The relaxed m-Hf(Zr)O_2 unit cell parameters are $a = 5.146(5.219)$ Å, $b/a = 1.010(1.012)$, $c/a = 1.036(1.036)$, and $\beta = 99.68°(99.68°)$, close to experimental values [23]: $a = 5.117(5.151)$ Å, $b/a = 1.011(1.010)$, $c/a = 1.034(1.032)$, and $\beta = 99.22°(99.20°)$. The formation enthalpy of m-Hf(Zr)O_2 calculated with respect to hcp Hf (Zr) and an isolated O_2 molecule is $-1166(-1106)$ kJ/mol, after adopting (throughout this Letter) the 1.36 eV energy correction for the O_2 molecule provided by Wang *et al.* [24].

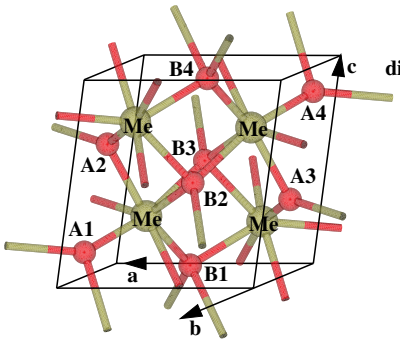

All inequivalent dioxygen-vacancy sites

(A1, A2)	(A1, B3)
(A1, A3)	(A2, B2)
(A1, A4)	(B1, B2)
(A1, B1)	(B1, B3)
(A1, B2)	(B2, B3)

FIG. 1 (color online). Unit cell used for calculations of the formation energy of oxygen vacancies in MeO_2 (Me = Hf or Zr) with all metal and oxygen sites identified. The ten inequivalent pairs of oxygen sites are also listed.

These results are in accordance with the experimental values, which are -1145 kJ/mol for hafnia and -1101 kJ/mol for zirconia [25].

We look for a conductive state in m-Hf(Zr)O_2 by increasing the concentration of oxygen vacancies in the materials. To serve as a reference, we first calculated the formation energies of single and double oxygen vacancies in a 96-atom m-Hf(Zr)O_2 supercell ($2 \times 2 \times 2$). Only the neutral oxygen vacancy was considered since our ultimate goal is an energetically favorable metallic phase, where charged point defects are not stable. There are two inequivalent O sites regarding O coordination, namely, the 3- and 4-coordinated O(A) and O(B) sites, respectively. The formation energy of a neutral oxygen vacancy is defined as

$$E_{\text{form}} = E_D - E_0 + \mu_{\text{O}}, \tag{1}$$

where E_D is the energy of the defective supercell, E_0 is the energy of the defect-free supercell, and μ_{O} is the chemical potential of oxygen. Under oxygen-rich conditions, μ_{O} is usually set as one-half of that of an O_2 molecule. In this case the calculated E_{form} for a neutral O(A) vacancy in m-Hf(Zr)O_2 is 7.13(6.62) eV, while for a neutral O(B) vacancy it is 7.00(6.53) eV. The difference between the two formation energies, 0.13(0.09) eV, is similar to Zheng *et al.* [26], but larger than Foster *et al.* who reported a 0.02 eV difference in both cases [27,28]. Next we calculated the formation energies of dioxygen-vacancy pairs in m-Hf(Zr)O_2. To this end, the eight oxygen sites in a unit cell were named $A1$–$A4$ and $B1$–$B4$, as shown in Fig. 1. The distance between two dioxygen-vacancy pairs is around 10 Å, casting them as isolated pairs. Since m-Hf(Zr)O_2 possesses the baddeleyite structure with space group $P2_1/c$, there are ten inequivalent dioxygen-vacancy pairs. The most energetically favorable pair is ($B1$, $B2$), whose formation energy per vacancy is the same as of a single O(B) vacancy.

Under usual experimental conditions the dielectric is placed between two metal electrodes where oxygen can migrate as an interstitial. We thus calculated the incorporation energies of oxygen, starting from its molecular form, into bulk hcp Ti and fcc Pt, two commonly used electrodes. The results are -6.24 and 0.91 eV, respectively. In Table I we compare the formation energies of isolated single and double oxygen vacancies in m-Hf(Zr)O_2 resulting in the release of O_2 or the incorporation of O interstitial in the two metals. Notice that the formation energy of a neutral O(B) vacancy in m-Hf(Zr)O_2 plus an oxygen interstitial in hcp Ti is merely 0.76(0.29) eV, which is attributed to the strong Ti-O bonding.

Next, O-deficient Hf(Zr)O_x with different stoichiometries were studied in the search for the dielectric-metal transition. We began with the Hf(Zr)$_4O_7$ models generated by introducing one oxygen vacancy per 12-atom

TABLE I. Formation energies of isolated single oxygen vacancies and dioxygen-vacancy pairs, and of substoichiometric Hf(Zr)$_4O_7$ and Hf(Zr)$_2O_3$, in different structures derived from monoclinic HfO_2 and ZrO_2. Me stands for Hf (Zr).

Chemical formula	Vacancy site(s)	Supercell units	Formation energy (eV/vacancy) with oxygen going to O_2	Ti	Pt
		Single oxygen vacancy			
$Me_{32}O_{63}$	O(A)	$2 \times 2 \times 2$	7.13(6.62)	0.89(0.38)	8.04(7.53)
$Me_{32}O_{63}$	O(B)	$2 \times 2 \times 2$	7.00(6.53)	0.76(0.29)	7.91(7.44)
		Closest dioxygen vacancy			
$Me_{32}O_{62}$	($B1$, $B2$)	$2 \times 2 \times 2$	7.01(6.52)	0.77(0.28)	7.92(7.43)
$Me_{32}O_{62}$	($B2$, $B3$)	$2 \times 2 \times 2$	7.02(6.60)	0.78(0.36)	7.93(7.51)
$Me_{32}O_{62}$	($A1$, $B1$)	$2 \times 2 \times 2$	7.03(6.53)	0.79(0.29)	7.94(7.44)
		Me_4O_7			
Me_4O_7	O(A)	$1 \times 1 \times 1$	7.16(6.66)	0.92(0.42)	8.07(7.57)
Me_4O_7	O(B)	$1 \times 1 \times 1$	7.03(6.57)	0.79(0.33)	7.94(7.48)
		Me_2O_3			
Me_4O_6	($B1$, $B2$)	$1 \times 1 \times 1$	6.55(5.66)	0.31(-0.58)	7.46(6.57)
Me_4O_6	($A1$, $B1$)	$1 \times 1 \times 1$	6.92(6.40)	0.68(0.16)	7.83(7.31)
Me_4O_6	($B2$, $B3$)	$1 \times 1 \times 1$	6.95(6.33)	0.71(0.09)	7.86(7.24)

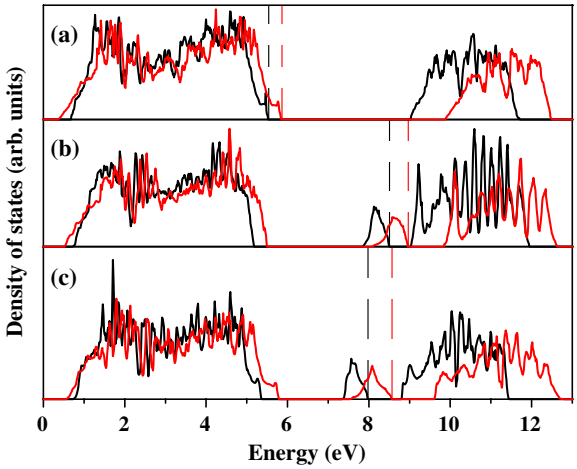

FIG. 2 (color online). DOS for (a) m-Hf(Zr)O_2, (b) Hf(Zr)$_4$O$_7$ with one O(A) vacancy, (c) Hf(Zr)$_4$O$_7$ with one O(B) vacancy. Black curves are for Zr-based compounds while gray (red) curves are for Hf-based compounds. All figures are aligned horizontally with respect to the O 2s band (not shown). The highest occupied molecular orbital levels are indicated by vertical dashed lines.

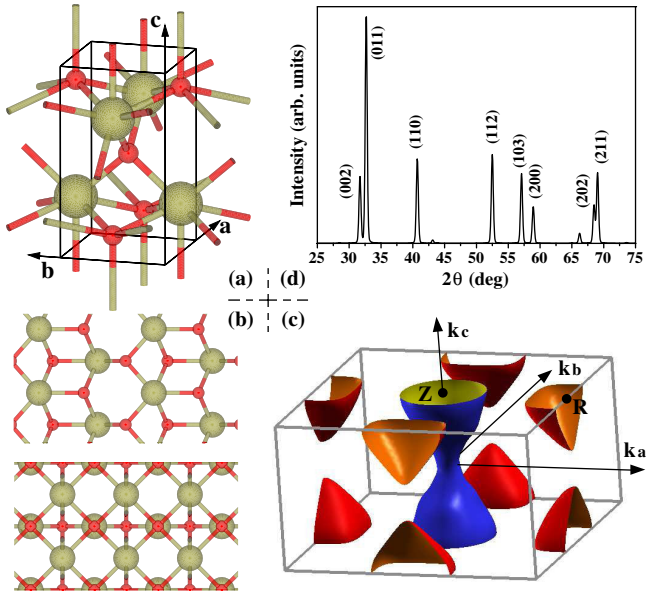

FIG. 3 (color online). Tetragonal Hf_2O_3 and Zr_2O_3 [38]. (a) Primitive cell with 5 atoms, (b) view along a axis (upper) and c axis (lower), (c) Fermi surface of Hf_2O_3 at $T = 0$ K, (d) simulated powder x-ray diffraction patterns of Hf_2O_3. Big green balls, Hf or Zr; small red balls, O.

m-Hf(Zr)O_2 for two inequivalent cases, i.e., O(A) and O(B). The defective unit cells were fully relaxed until all Hellmann-Feynman forces were less than 0.01 eV/Å. Atomic coordinates, cell dimensions, and shape were subject to relaxation. The formation energies per vacancy of the two Hf(Zr)$_4$O$_7$ phases are almost the same as in the single oxygen vacancy cases. The resulting densities of states (DOS) are shown in Figs. 2(b) and 2(c). The calculated band gaps are similar to m-Hf(Zr)O_2 [Fig. 2(a)], around 4.0(3.5) eV compared with experimental values 5.8(5.4) eV [29,30]. Since the band gap is underestimated by GGA, a more accurate calculation employing many-body techniques can only push Hf(Zr)$_4$O$_7$ even farther from a metal. Moreover, Figs. 2(b) and 2(c) show that a fully occupied defect-induced band emerges in the band gap which cannot account for the measured metallic state in hafnia-based RRAM where the resistance is on the order of hundreds of ohms for 10 nm thick films [31]. However, the trend does hint at a possible dielectric-to-metal phase transition for stronger off-stoichiometric hafnia or zirconia.

Hence, several Hf(Zr)$_2$O$_3$ models were set up with two oxygen vacancies per 12-atom m-Hf(Zr)O_2 unit cell. For all inequivalent cases (Fig. 1) the cells remain monoclinic during relaxation of the unit cell vectors, except for the ($B1$, $B2$) case which suffers from a monoclinic-to-tetragonal transition. The tetragonal Hf(Zr)$_2$O$_3$ [t-Hf(Zr)$_2$O$_3$] phase (Fig. 3; structural parameters in Table II) is the ground state of all ten Hf(Zr)$_2$O$_3$ candidates. It belongs to the D_{2d} point group and $P\bar{4}m2$ (No. 115) space group [32]. Symmetry analysis indicates that Hf(Zr) and 2/3 of the oxygen sites [named O(A)] are at the 2g position while 1/3 of the oxygen sites [named O(B)] are at the 1c position [33]. The Hf(Zr) coordination number is 7 as in m-Hf(Zr)O_2, while O(A) and O(B) have coordination numbers 5 and 4, respectively. The average Hf(Zr)-O(A) and Hf(Zr)-O(B) bond lengths are 2.295(2.322) and 2.089(2.134) Å, respectively, compared with 2.084(2.117) and 2.209(2.240) Å in m-Hf(Zr)O_2. Bader analysis reveals less charge transfer from Hf(Zr) to O in t-Hf(Zr)$_2$O$_3$ than in m-Hf(Zr)O_2. The Hf(Zr) charge changes from 2.73e(2.57e) in m-Hf(Zr)O_2 to 2.10e(2.02e) in t-Hf(Zr)$_2$O$_3$; the O(A) charge changes from $-1.34e(-1.25e)$ to $-1.39e(-1.34e)$; and the O(B) charge changes from $-1.39e(-1.31e)$ to $-1.41e(-1.37e)$.

Figure 4 shows the band diagram and orbital-projected DOS of t-Hf_2O_3. Results for t-Zr_2O_3 (not shown) are similar. The high symmetry points in the Brillouin zone are named according to the Bilbao crystallographic server [32]. A semimetallic behavior is revealed in the overlap of the partially occupied valence band top and conduction band bottom located at the different high symmetry points R and Z, respectively. Both band edges are mostly derived from Hf 5d states. The semimetallic character of the two compounds was confirmed by G_0W_0 calculations of the many-body correction to the GGA energy levels. As shown

TABLE II. Calculated structural parameters of tetragonal Hf_2O_3 and Zr_2O_3.

	a	c	Hf$_z$	O(A)$_z$	Bulk modulus
Hf_2O_3	3.135 Å	5.646 Å	0.2553	0.1351	246 GPa
Zr_2O_3	3.174 Å	5.763 Å	0.2525	0.1367	228 GPa

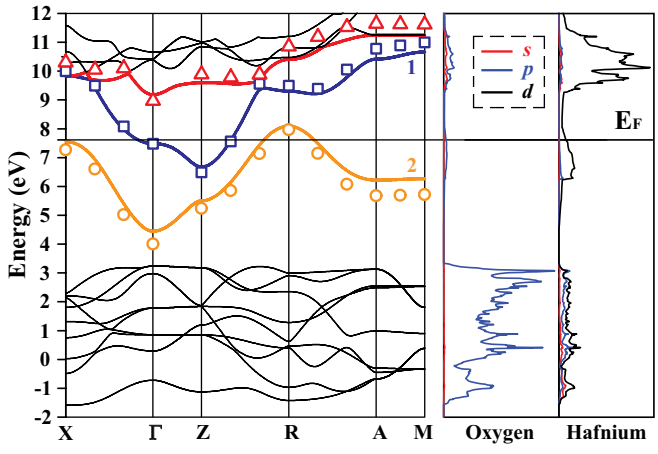

FIG. 4 (color online). Tetragonal Hf_2O_3 electronic band structure (left) and orbital projected DOS (right). DFT-GGA (solid lines) and G_0W_0 (discrete marks) band structures are superimposed and aligned by their Fermi levels. Results for tetragonal Zr_2O_3 (not shown) are similar.

in Fig. 4, the energy shifts are small, of the order of a few tenths of eV. From the calculated band structures the densities of conduction electrons and holes can be obtained by integrating their occupation of the blue (No. 1) and orange (No. 2) bands shown in Fig. 4, respectively. The electron and hole densities are both 1.8×10^{21} cm^{-3}, below 10^{22} cm^{-3} which sets the upper limit for semimetals, but substantially larger than common semimetals such as Bi, Sb, and As, with carrier concentrations 3×10^{17}, 5×10^{19}, and 2×10^{20} cm^{-3}, respectively [34]. The same concentration of electrons and holes indicates a band-to-band transfer mechanism, pointing to a typical compensated semimetal. The Fermi surface of t-Hf_2O_3 is plotted in Fig. 3(c), showing conduction electrons near the Z and Γ points, as well as holes near the R point.

To evaluate the relative stability of this structure, we calculated the molar formation enthalpy of various Hf_2O_3, Zr_2O_3, and Ti_2O_3 models with respect to their corresponding metals and O_2. The formation enthalpy of t-$Hf(Zr)_2O_3$ is $-1700(-1666)$ kJ/mol, more favorable than fully relaxed corundum $Hf(Zr)_2O_3$, $-1586(-1580)$ kJ/mol. The chemical transformation from t-$Hf(Zr)_2O_3$ to m-$Hf(Zr)O_2$ can be written as

$$Hf_2O_3 + \tfrac{1}{2}O_2 \rightleftharpoons 2HfO_2 + 632 \text{ kJ} \quad (2)$$

and

$$Zr_2O_3 + \tfrac{1}{2}O_2 \rightleftharpoons 2ZrO_2 + 546 \text{ kJ}, \quad (3)$$

respectively. On the other hand, the formation enthalpy of fully relaxed Ti_2O_3 arranged in the $P\bar{4}m2$ tetragonal structure is -1576 kJ/mol, less favorable than corundum Ti_2O_3 whose formation enthalpy is -1598 kJ/mol. These results indicate that while the tetragonal $P\bar{4}m2$ structure is preferred over corundum for $Hf(Zr)_2O_3$, the opposite is true for Ti_2O_3.

To our best knowledge, the proposed t-Hf_2O_3 and t-Zr_2O_3 structures have not been reported before, though some experimental data may suggest their existence. Hildebrandt *et al.* [35] performed high-resolution transmission electron microscopy of a conducting HfO_{2-x} thin film where the enlarged inverse Fourier-transformed images show a similar structure as in Fig. 3(b). Manory *et al.* [36] discovered two unidentified x-ray diffraction (XRD) peaks at $2\theta = 40°$ and $2\theta = 52°$ in hafnia films grown by ion beam assisted deposition at a transport ratio of 5 and an ion energy of 20 keV. They attributed these peaks to a new tetragonal structure and suggested the Hf_2O_3 stoichiometry. However, they simulated their data with a $P4/mmm$ phase with lattice parameters $a = 5.055$ Å and $c = 5.111$ Å, resulting in two small peaks around 40°. We calculated powder XRD patterns [37] for t-Hf_2O_3 [Fig. 3(d)] using Cu $K\alpha$ radiation ($\lambda = 1.5418$ Å), and found a (110) peak at 40.7° and a (112) peak at 52.5°, close to data. A similar calculation for t-Zr_2O_3 yielded a (110) peak at 40.2° and a (112) peak at 51.6°.

In conclusion, we have predicted tetragonal semimetallic Hf_2O_3 and Zr_2O_3 structures as the ground state of highly oxygen deficient hafnia and zirconia which undergo a monoclinic-to-tetragonal phase transition. Their semimetallic properties are characterized by an overlap of the valence band maximum and conduction band minimum at different points of the Brillouin zone, and by low densities of conduction electrons and holes. The presence of t-Hf_2O_3 in O-deficient electroformed HfO_x is a possible explanation of the conductive state of hafnium-based RRAM.

We especially thank Dr. Blanka Magyari-Köpe from Stanford University for pointing out the experimental results in Ref. [36]. This work is financially supported by the Nanosciences Foundation of Grenoble (France) in the frame of the Chairs of Excellence awarded to L. R. C. F. and to Y. N. L. R. C. F. also acknowledges CNPq for financial support. The calculations were performed on the Stanford NNIN (National Nanotechnology Infrastructure Network) Computing Facility funded by the National Science Foundation (U.S.A.).

[1] S. Lange, V. Kiisk, V. Reedo, M. Kirm, J. Aarik, and I. Sildos, Opt. Mater. **28**, 1238 (2006).
[2] J. A. Kilner, Nat. Mater. **7**, 838 (2008).
[3] J. Robertson, Rep. Prog. Phys. **69**, 327 (2006).
[4] A. Asamitsu, Y. Tomioka, H. Kuwahara, and Y. Tokura, Nature (London) **388**, 50 (1997).
[5] S. Q. Liu, N. J. Wu, and A. Ignatiev, Appl. Phys. Lett. **76**, 2749 (2000).
[6] R. Waser and M. Aono, Nat. Mater. **6**, 833 (2007).
[7] B. Magyari-Köpe, M. Tendulkar, S.-G. Park, H. D. Lee, and Y. Nishi, Nanotechnology **22**, 254029 (2011).
[8] D.-H. Kwon, K. M. Kim, J. H. Jang, J. M. Jeon, M. H. Lee, G. H. Kim, X.-S. Li, G.-S. Park, B. Lee, S. Han, M. Kim, and C. S. Hwang, Nat. Nanotechnol. **5**, 148 (2010).

[9] K.-L. Lin, T.-H. Hou, J. Shieh, J.-H. Lin, C.-T. Chou, and Y.-J. Lee, J. Appl. Phys. **109**, 084104 (2011).

[10] K. Kamiya, M. Y. Yang, S.-G. Park, B. Magyari-Köpe, Y. Nishi, M. Niwa, and K. Shiraishi, Appl. Phys. Lett. **100**, 073502 (2012).

[11] P. Hohenberg and W. Kohn, Phys. Rev. **136**, B864 (1964); W. Kohn and L. J. Sham, Phys. Rev. **140**, A1133 (1965).

[12] G. Kresse and J. Furthmüller, Comput. Mater. Sci. **6**, 15 (1996); Phys. Rev. B **54**, 11169 (1996).

[13] P. E. Blöchl, Phys. Rev. B **50**, 17953 (1994); G. Kresse and D. Joubert, Phys. Rev. B **59**, 1758 (1999).

[14] J. P. Perdew, K. Burke, and M. Ernzerhof, Phys. Rev. Lett. **77**, 3865 (1996).

[15] H. J. Monkhorst and J. D. Pack, Phys. Rev. B **13**, 5188 (1976).

[16] M. S. Hybertsen and S. G. Louie, Phys. Rev. B **30**, 5777 (1984).

[17] P. Broqvist, A. Alkauskas, and A. Pasquarello, Phys. Rev. B **78**, 075203 (2008).

[18] L. Hedin, Phys. Rev. **139**, A796 (1965).

[19] F. Bruneval, N. Vast, and L. Reining, Phys. Rev. B **74**, 045102 (2006).

[20] The DFT-GGA band structures obtained with the VASP and ABINIT codes differ by less than 10 meV, justifying the application of ABINIT G_0W_0 energy shifts to the VASP eigenvalues.

[21] N. Troullier and J. L. Martins, Phys. Rev. B **43**, 1993 (1991).

[22] R. W. Godby and R. J. Needs, Phys. Rev. Lett. **62**, 1169 (1989).

[23] R. E. Hann, P. R. Suitch, and J. L. Pentecost, J. Am. Ceram. Soc. **68**, C-285 (1985).

[24] L. Wang, T. Maxisch, and G. Ceder, Phys. Rev. B **73**, 195107 (2006).

[25] J. G. Speight, *Lange's Handbook of Chemistry* (McGraw-Hill, New York, 2004), 16th ed.

[26] J. X. Zheng, G. Ceder, T. Maxisch, W. K. Chim, and W. K. Choi, Phys. Rev. B **75**, 104112 (2007).

[27] A. S. Foster, V. B. Sulimov, F. Lopez Gejo, A. L. Shluger, and R. M. Nieminen, Phys. Rev. B **64**, 224108 (2001).

[28] A. S. Foster, F. Lopez Gejo, A. L. Shluger, and R. M. Nieminen, Phys. Rev. B **65**, 174117 (2002).

[29] N. V. Nguyen, A. V. Davydov, D. Chandler-Horowitz, and M. M. Frank, Appl. Phys. Lett. **87**, 192903 (2005).

[30] M. Houssa, M. Tuominen, M. Naili, V. Afanas'ev, A. Stesmans, S. Haukka, and M. M. Heyns, J. Appl. Phys. **87**, 8615 (2000).

[31] C. Cagli *et al.*, in *2011 IEEE International Electron Devices Meeting*, Technical Digest (IEEE, New York, 2011), p. 28.7.1.

[32] M. I. Aroyo, J. M. Perez-Mato, C. Capillas, E. Kroumova, S. Ivantchev, G. Madariaga, A. Kirov, and H. Wondratschek, Z. Kristallogr. **221**, 15 (2006).

[33] http://www.cryst.ehu.es/cgi-bin/cryst/programs/nph-wp-list?gnum=115.

[34] N. W. Ashcroft and N. D. Mermin, *Solid State Physics* (Saunders College Publishing, Philadelphia, PA, 1976).

[35] E. Hildebrandt, J. Kurian, M. M. Müller, T. Schroeder, H.-J. Kleebe, and L. Alff, Appl. Phys. Lett. **99**, 112902 (2011).

[36] R. R. Manory, T. Mori, I. Shimizu, S. Miyake, and G. Kimmel, J. Vac. Sci. Technol. A **20**, 549 (2002).

[37] J. Rodríguez-Carvajal, Physica (Amsterdam) **192B**, 55 (1993).

[38] Structures drawn by VESTA, K. Momma and F. Izumi, J. Appl. Crystallogr. **44**, 1272 (2011); Fermi surface drawn by XCrySDen, A. Kokalj, Comput. Mater. Sci. **28**, 155 (2003).